Optical Materials 111 (2021) 110575

Contents lists available at ScienceDirect

Optical Materials

journal homepage: http://www.elsevier.com/locate/optmat

Design of tunable liquid laser based on presence of the conjugated-polymer counter influencing the spectral properties of the oligomer

Mamduh J. Aljaafreh [a], Mohamad S. AlSalhi [a,b,*], Saradh Prasad [a,b]

[a] Department of Physics and Astronomy, College of Science, King Saud University, 11451, Riyadh, Saudi Arabia
[b] Research Chair on Laser Diagnosis of Cancers, Department of Physics and Astronomy, College of Science, King Saud University, 11451, Riyadh, Saudi Arabia

ARTICLE INFO

Keywords:
Dual amplified spontaneous emission (ASE)
Absorption modification
Appearance of new ASE peak
Tunable laser
Time-resolved spectroscopy (TRS)

ABSTRACT

In this paper, we studied the optical properties, lasing properties, and time-resolved spectroscopy (TRS) dynamics of the energy transfer between the conjugated oligomer (CO) 1,4-bis(9-ethyl-3-carbazo-vinylene)-9,9-dihexyl-fluorene (BECV-DHF) and conjugated-polymer (CP) influencer poly[2-methoxy-5-(2′-ethylhexyloxy)-1,4-phenylene vinylene] (MEH-PPV) in a toluene environment. The oligomer 1,4-bis(9-ethyl-3-carbazo-vinylene)-9,9-dihexyl-fluorene (BECV-DHF) exhibits single amplified spontaneous emission (ASE) in a solution for a wide variety of concentration and solvent environment, but it produces dual ASE under the influence of MEH-PPV. The dual ASE of the oligomer is due to the interaction between these two laser materials, and it is studied using various spectroscopic techniques. The TRS showed that the presence of the CP in the CO solution does not change the excited state dynamics of the CO, and the fluorescence of the CO is quenched, and the fluorescence of CP is enhanced simultaneously; hence, the underlying mechanism could be modulation of the absorption band at specific wavelength region (460 ± 10 nm). Under an optical cavity (100%–60% reflectivity plane mirrors and with internal grating), a tunable laser with a 6 nm full width at half maximum (FWHM) from 560 nm to 580 nm and attenuation from 600 to 650 nm was observed. Spectrally narrow peaks were obtained at various wavelengths by changing the cavity mirror distance. This strategy of obtaining a laser tunable from 560 to 580 nm, in addition to dual ASE (436 nm and 464 nm), from a CP and CO blend could potentially facilitate the development of an efficient, low-cost laser.

1. Introduction

Conjugated oligomers (COs) are relatively new materials often ignored in favor of regular conjugated polymers and other molecules. Nevertheless, they have advantageous properties of small molecules, such as easy solubility and synthesis, high scalability, robust photophysical and photochemical properties, and inherit the desirable properties of conjugated polymers, such as flexibility and self-assembly [1–3]. The spectroscopic and optoelectronic properties of CPs have been extensively studied, and their applications are widespread in many fields, such as biomedicine [4,5], defense [6] and aerospace [7], and in optoelectronic devices, such as lasers, energy storage devices, sensors, and light-emitting diodes [8–17]. Similarly, COs have been found to be useful in many efficient devices, such as optically pumped lasers, photovoltaic devices, and sensors [18–25]. A new synthesis of co-oligomers with lasing properties that can be tuned throughout the visible spectrum is ongoing research. Thiophene phenyl co-oligomers are found to produce lasers in single crystal form with high efficiencies [26].

The photophysical properties, such as absorption, fluorescence, quantum yield, and energy transfer process, of oligomers, have been extensively studied. However, the oligomer BECV-DHF is relatively new. In general, a CO has a very high quantum yield and a high stimulated emission coefficient; hence, it is considered an efficient material in transferring energy. In general, the energy transfer between chromophores can occur through three different mechanisms. The first, which occurs over a very short range (distance < 10 Å), is called the Dexter type. It is a nonradiative energy transfer, including fluorescence quenching, where the two molecules exchange their electrons. The second type is Förster resonance energy transfer (FRET), which is a nonradiative process from a donor molecule to an acceptor molecule without emission of a photon. It occurs due to dipole-dipole interactions, in which the distance between the donor and acceptor should be in the range of 10–100 Å (Angstrom). The third is long-range dipole-dipole

* Corresponding author. Department of Physics and Astronomy, College of Science, King Saud University, 11451, Riyadh, Saudi Arabia.
E-mail address: malsalhi@ksu.edu.sa (M.S. AlSalhi).

https://doi.org/10.1016/j.optmat.2020.110575
Received 11 August 2020; Received in revised form 19 October 2020; Accepted 21 October 2020
Available online 31 October 2020

energy transfer (LFRET), where the distance between the acceptor and donor can be greater than 100 Å but less than 150 Å. This mechanism does not require any dipole or orbital interaction between A and D, so it can occur over a large distance [25].

Previously, FRET was found to be a mechanism between conjugated materials. Additionally, energy transfer between quantum dots and MEH-PPV through the Dexter energy transfer type has been demonstrated [27]. This was proven through measurement of the rate of change in the absorption and fluorescence rate over time, where the quenching reached a maximum and then decreased. Radiative-type energy transfer between a CO and a CP was observed using time-resolved spectroscopy by Parasd et al. [25]. The energy transfer between the water-soluble trimethylalkyammonium group and water-soluble cationic oligomers was considered to be FRET. The distance between the donor and acceptor is critical to the energy transfer efficiency [28]. A. Heeger et al. showed that a few water-soluble oligomers had a good spectral overlap between D and A; hence, FRET is efficient between them [29]. A time-integrated three-plus stimulated echo peak shift (3PEPS) experiment was utilized to investigate the energy transfer between the CP MEH-PPV and polymer pom-DEHOMSSB, and the results showed that the interplay of conjugation and conformation disorder gives rise to the optical properties of the CP, which are quite different from those of normal molecular dyes [30]. Intrachain energy transfer between organometallic co-oligomers and polymers was studied. The results showed that energy transfer occurs through possible triplet sites [31].

S. Dineshkumar et al. designed mesoporous oligomers with aggregation-induced enhanced emission (AIEE) properties. The enhanced energy transfer between the conjugated mesoporous oligomer and picric acid was attributed to the larger pore size and pore density in the mesoporous network of the mesoporous oligomer. This property was used for sensing trace amounts of nitroaromatic compounds for explosives detection [32]. Similarly, intramolecular energy transfer of the FRET type was used to detect 2,4,6-trinitrotoluene (TNT) using a fluorescence dye and an organic amine at the surface of silica nanoparticles [33].

Azobenzene-based materials are very versatile and robust. It found a wide range of applications [34,35], especially it has unique optical nonlinear and laser properties that rival ordinary conjugated polymer materials. In laser, Azobenzene-based materials produced a tunable laser using distributed feedback configuration (DFB) with a 200 nm spectral tunability range in the red and IR region [36]. A copolymer made using poly (methyl methacrylate) (PMMA) and azo-monomer was found to be efficient in the second harmonic generation [37]. A complete series of azobenzenes substituted with 2,4-nitro/cyan moieties were investigated for its nonlinear optical properties. The result showed the formation of table Z isomers in N, N0 –dimethylformamide solution. The Z isomers have potential applications in optical data storage. These materials showed high thermal relaxation rate values in toluene, which have potential optical switching applications [35]. NMR, FTIR, and quantum chemical calculations of nitro/cyano mono and disubstituted azo-monomers show that fast thermal relaxation is due to the substitution pattern azo-moieties [38]. Simultaneous two and three-photon resonances and third-order nonlinear optical susceptibility are efficiently and stability produced by a polymer (PMMA-M3, poly (4-((2-cyano-4-nitrophenyl) diazenyl)phenyl methacrylate-co-methyl methacrylate)) [39].

Both CPs and COs are exceptional laser materials and produce lasers at an appropriate concentration in many solvents and thin films. COs have specified molecular weight and better control of molecular structures. In this study, we utilize a blue-emitting oligomer and a red-emitting polymer to study the interaction between them. We show that the CP can also influence the photophysical properties of the CO. The combination of MEH-PPV and BECV-DHF increases the quantum efficiency and stability of both when compared to the individual solution. It could lead to the design of efficient optoelectronic devices such as thin-film laser, OLED, and OFETs. The presence of MEH-PPV affects and modulates the spectral and ASE properties of the CO and forces the CO to produce dual ASE, which is impossible for the pure CO in solution. Furthermore, utilizing this composite solution in an optical cavity system, the broadband at 550–610 nm was converted to a tunable laser with a divergence of 15 mrad.

2. Materials and methods

The CP MEH-PPV and CO BECV-DHF with molecular masses of 100,000 g mol^{-1} and 773.12 g mol^{-1}, respectively, were used in this study. These materials were obtained from the American Dye Source (Montreal, Quebec, Canada) and used without any treatment as received. The molecular structures of BECV-DHF and MEH-PPV are presented in Fig. 1 (a) and (b). The relative concentration of the two materials in the blends has been changed by mixing proper amounts of the CO and the MEH-PPV toluene solutions [40]. To measure the spectral characteristics and laser properties of the solutions of these materials, the following experimental setup was used. A quartz cuvette (1 cm × 1 cm × 4 cm) and an optical path length of 10 mm were used. Absorption spectra and fluorescence spectra were obtained using a Perkin-Elmer Lambda 950 spectrophotometer (Llantrisant, United Kingdom) and a Perkin-Elmer LS-55 spectrofluorometer, respectively. The simulation study was done using TD-DFT with the B3LYP/6-31G* (d,p) basis sets using Gaussian software [41]; the molecules were kept in toluene cavitation.

The pump source was a 355 nm Nd:YAG laser (Les Ulis, France) with a pulse duration of 5–10 ns and a repetition rate of 10 Hz. To achieve transverse excitation of samples, a 5 cm focal length quartz plano-convex lens functioned to focus the UV pulsed laser into the samples. The tunable laser arrangement was made two ultrafast mirrors 100% and 60% reflectivity, with a grating 1000 line/inch in before 60% output mirror. The output emission, ASE, and laser were fed to a PI MAX 4 ultrafast camera (Princeton Instruments with an Acton spectrograph) through an optical fiber. The ultrafast camera had an actively gated emCCD with a gate time of 400 ps. Another fiber was utilized to feed the emission output to a spectrometer equipped with a linear array charge-coupled device (CCD) [Ocean Optics Spectroscopy, USB4000-XR1-ES].

3. Results and discussion

3.1. Optical properties of the pure CO and CP

The absorption and fluorescence spectra of the CO are shown in Fig. 2. The absorption spectrum shows a shoulder at approximately 375 nm and two peaks at 398 nm and 420 nm, whereas fluorescence peaks are observed at 441.5 nm and 466 nm with a shoulder at 495.5 nm. Note that the CO produces ASE only at approximately 464 nm in solution, even at the minimum concentration at which ASE is achievable.

Fig. 3 (a) shows the absorption spectrum for the CP MEH-PPV. Two peaks are observed at approximately 500 nm and 332 nm, with a wide gap of 188 nm between them. The simulation of the absorption spectrum of MEH-PPV (4 unit approximation) was done using TD-DFT with the B3LYP/6-31G* (d,p) basis sets and in toluene cavitation. The theoretically simulated value of λ_{max} at 470 nm showed a strong agreement with the experimental λ_{max} at 500 nm with a 30 nm difference, as shown in Fig. S1. Fig. 3 (b) displays the normalized fluorescence spectra of the CP at different concentrations. The major peaks redshift and change with increasing concentration. The peaks at 567 nm and 598 nm are due to the 0-0 and 0–1 vibrational transitions.

Fig. 4 (a) presents the absorption spectra of CO/CP composite solutions at ratio (1:0.4) as well as pure CO and CP. The CO has the same peak positions, whereas the CP has a broad absorption peak from 450 nm to 550 nm. The absorption spectra of both are superimposed constructively with a minimum around 420 nm, which coincides with 0–1 vibrational band of the pure CO. since the absorption of MEH-PPV in

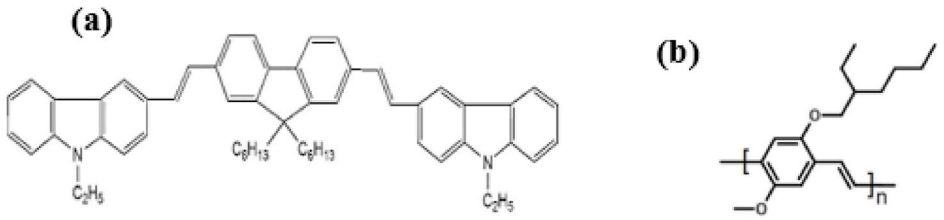

Fig. 1. Molecular structure of the (a) conjugated oligomer BECV-DHF and (b) conjugated polymer MEH-PPV.

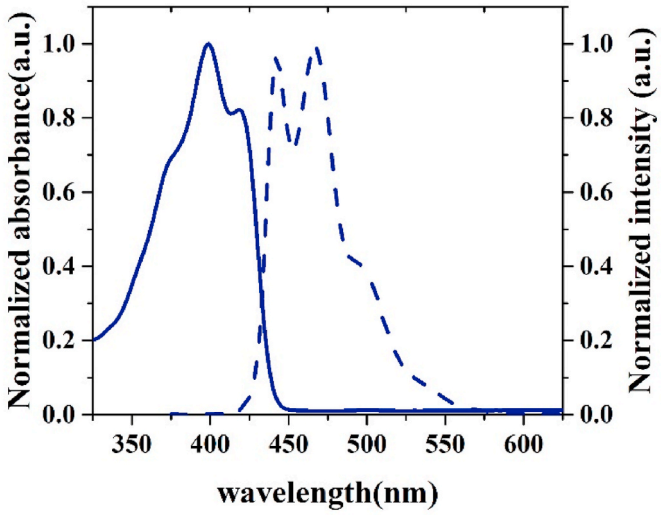

Fig. 2. Normalized absorption and fluorescence spectra of the CO at a concentration of 10 μg/ml in toluene.

this region is weak and it allows 0–1 transition of the oligomer to become dominant in fluorescence and ASE (as discussed in the latter part of this article). Note the increase in absorption of CO under the influence of MEH-PPV; this could to due the time of measurement is close to the time of sample preparation. Later the absorption of CO is quenched and stabilized; please see Fig. 5 (a). Fig. 4 (b) fluorescence spectrum of the materials composite in solution shows quenching of the CO peak when 50 μL of the CP is added. The fluorescence peak of the oligomer is quenched to approximately 80% of the original strength. The coincidence of the fluorescence band with the absorption minima at 441 nm is very strong evidence for modulation in the HOMO-LUMO structure.

The absorption spectra of the CP and CO at different times (minutes) were measured to investigate the reaction between the CP and CO and are plotted in Fig. 5 (a). The inset in Fig. 5 (a) shows the absorbance at the 400 and 506 nm peaks with respect to time. Initially, when no MEH-PPV is present, the peak absorbance is 1.6 (a.u.). At 2 min after the addition of CP molecules (50 μL), the absorbance of the CO increases slightly, and the peak of the MEH-PPV also rises but at a much faster rate. At 24 min, the absorbance peaks at 440 nm, and 506 nm reach the maximum. At 30 min, the absorbance at 404 nm drops suddenly, whereas the absorbance at 506 nm decreases slightly. After this time, both of them maintain an almost constant absorbance.

In Fig. 5 (b), we study the fluorescence reaction of the composite. The fluorescence is quenched immediately after the introduction. At 2 min, the fluorescence is quenched to 50% of the initial intensity. The inset figure shows the fluorescence peak intensity with time. At approximately 10 min, the fluorescence drops to the minimum value of approximately 40% of the original value. The fluorescence intensity at 466 nm increases slightly up to 48% at approximately 30 min and then remains around the same intensity. Note that the intensity of the peak corresponding to MEH-PPV is unchanged since the concentration remains constant. The absorbance of the CP does not increase monotonically but attains a maximum at 30 min and then decreases slightly. The fluorescence quenching of the oligomer due to the presence of the CP is not monotonically increasing (decreasing intensity); at 10 min, it attains the lowest value of 40% of the original intensity. However, the intensity increases up to 48% after 30 min; the ratio between the oligomer peaks varies dramatically over time, as shown in Fig. 5 (a).

Fig. 5 (b) indicates that the minimum intensity appears at approximately 12 min, and the intensity ratio changes in the presence of the MEH-PPV, suggesting an energy transfer. A similar observation was made between PbS QD and MEH-PPV system by Y. Zhang et al. [27]. The increase, decrease and stabilization of blend solution absorption spectra indicated a permanent physical interaction between CO and CP. The simulation also shows the proximity of HOMO and HOMO+2 level of CO and CP. The modulation of absorption spectra is also observed experimentally. Modulation of absorption spectra occurred due to a change in the HOMO – LUMO structure of CO under the presence of MEH-PPV. In order to influence the HOMO - LUMO structure, the CO and CP must be close. The Dexter-type energy transfer is possible when CO and CP are closed. The TD-DFT calculation shows that LUMO of oligomer and LUMO+2 of MEH-PPV was very close with a gap of 80 meV (see Supplementary Fig. S2). Note, the literature and our calculations are in agreement. The LUMO level of the oligomer is −2.022 eV [19], which is

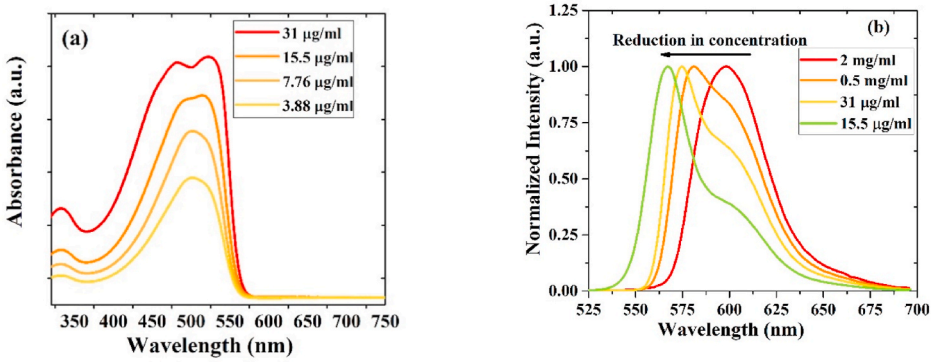

Fig. 3. (a) Absorption spectra and (b) fluorescence spectra of MEH-PPV at different concentrations in toluene.

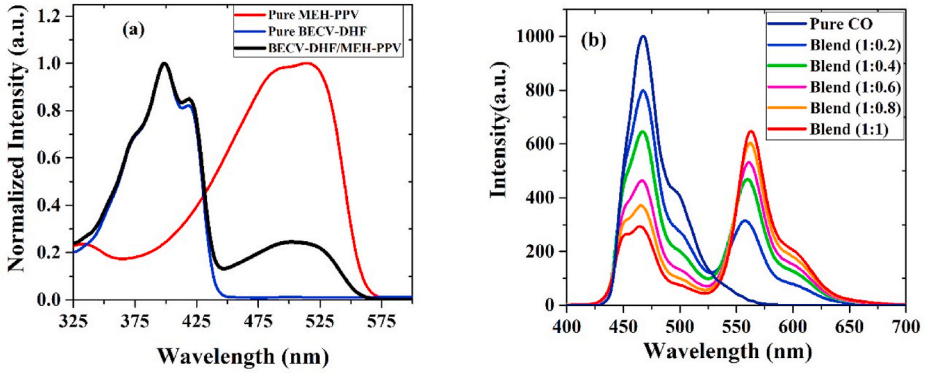

Fig. 4. (a) Absorption spectra for BECV-DHF, MEH-PPV and their blends. and (b) fluorescence spectra of the pure CO at 0.25 mg/ml and BECV-DHF/MEH-PPV blends with the same ratios. The ratios of BECV-DHF/MEH-PPV were 1:0.2, 1:0.4, 1:0.6, 1:0.8 and 1:1.

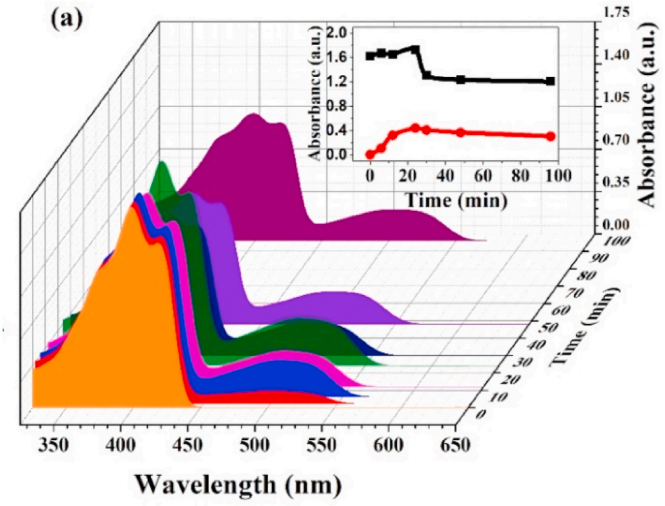

Fig. 5 (a). Absorption spectra of the CO/CP at a ratio of 1:0.2 at different reaction times.

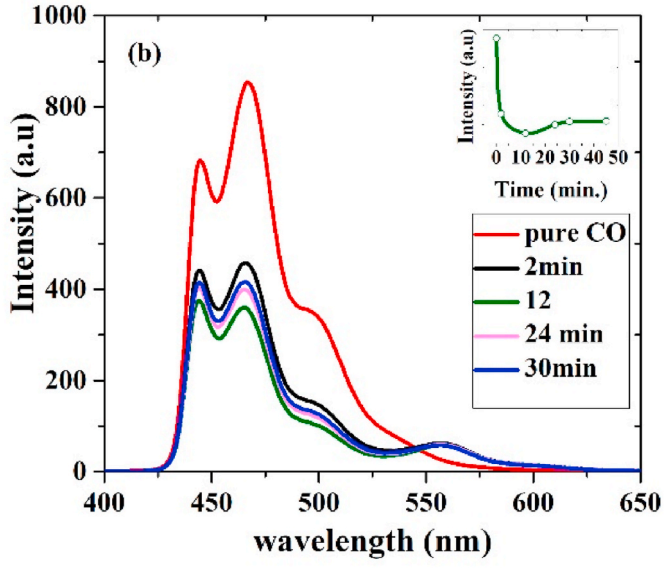

Fig. 5 (b). Fluorescence spectra of the CO/CP at a ratio of 1:0.2 at different reaction times.

678 meV above the LUMO of MEH-PPV (−2.700 eV) [42]. Even though there is a high overlap between the CO emission and CP absorption but still not enough evidence for Dexter energy transfer. But the above observation, along with the new ASE peak, can also be explained as follows, a CO ASE modulation is due to the MEH-PPV absorption at 464 nm. From the MEH-PPV absorption spectra (Fig. 4b), it is evident that the absorbance is higher at 464 nm than at 436 nm. Thus, in the presence of MEH-PPV, the absorption losses at 464 nm are increased more than the one at 436 nm, allowing this 436 nm peak to produce ASE (see ASE discussion). We are able to observe the influence of CP on CO; it could be most likely due to the modulation of absorption spectra and less likely involving Dexter energy transfer.

Fig. 6 (a) shows the ASE action from the pure CO at a concentration of 0.5 mg/ml. The pure oligomer produces ASE only at 464 nm for the minimum energy (4 mJ) and for the lowest concentrations in toluene below, which ASE is not possible. This oligomer does not produce dual ASE on its own, regardless of the pump energy, below this concentration, in contrast to some other COs [43] and CPs [44]. Fig. 6 (b) shows the ASE spectrum for pure MEH-PPV; here again, ASE is achieved at 605 nm without any other emitting species. However, in an earlier report, it was found that MEH-PPV could produce dual or triplet ASE under special conditions such as very high concentration and high pump energy or in the presence of quantum dots [45].

Fig. 7 shows the laser-induced fluorescence spectra of CO/CP blends at an 8 mJ pump energy and different concentrations of MEH-PPV except for the inset of Fig. 7 (b), where the pump energy is increased to 12 mJ. The concentration of MEH-PPV was increased in steps of 50 μL. Immediately after the addition of 50 μL of the CP to CO solution, a peak starts appearing at 436 nm, and the two peaks of MEH-PPV are visible at 565 nm and 603 nm. When the concentration of the CP is increased to 100 μL, the band at 436 nm becomes 50% of the band at 464 nm, as shown in Fig. 7 (b). The inset in Fig. 7 (b) clearly shows that when the pump energy is increased, the pump energy only increases the strength of the 436 nm peak since MEH-PPV is at a low concentration. The increase in pump energy did not improve the intensity of the MEH-PPV peak since it is already at maximum intensity. Fig. 7 (c) showed the LIF spectrum of the composite solution when the concentration of the CP was increased to 150 μL. The addition of the MEH-PPV increases the intensities of the oligomer band at 436 nm to 62% of the intensity of the 464 nm band, indicating dual ASE of the CO, and the broad LIF band of the CP with a 565 nm peak and a 603 nm shoulder, but MEH-PPV does not produce an ASE band. When the concentration of MEH-PPV is further increased to 200 μL, the intensity of the 436 nm peak of the CO becomes dominant, approximately 1.5 times that of the 464 nm peak. The strength of the 436 nm peak increases proportionally due to the increase of MEH-PPV concentration. The presence of MEH-PPV alters the vibrational equilibrium of the oligomer in the excited state, and both the 0–1 and 0–2 bands of the oligomer achieve population inversion and

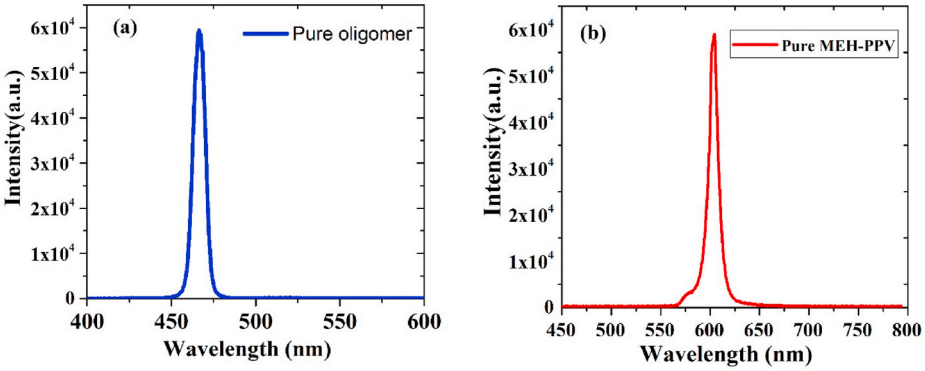

Fig. 6. (a) ASE spectrum of the CO in toluene, and (b) ASE spectrum of the CP in toluene.

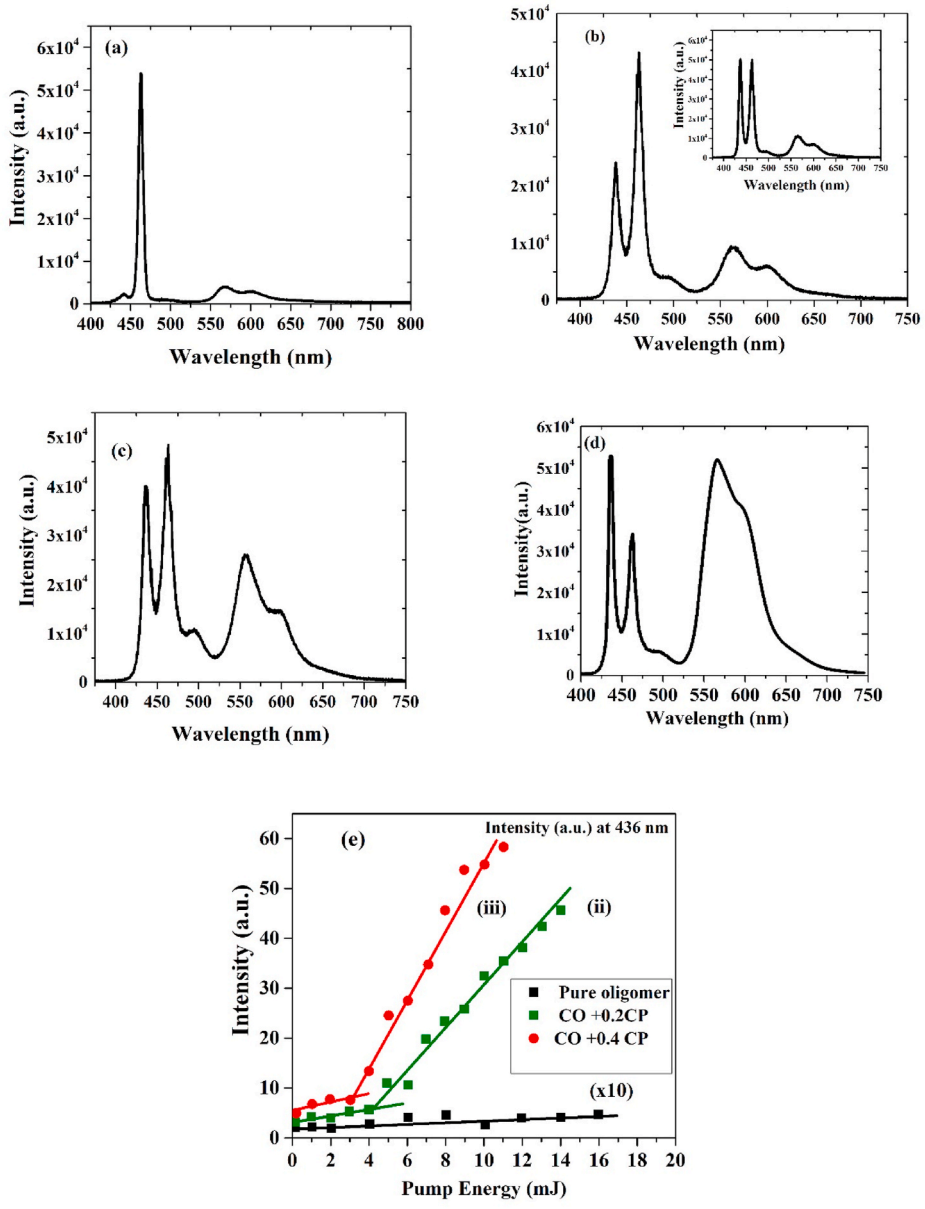

Fig. 7. (a) Combined ASE and LIF spectra of CO/CP blends in toluene with ratios of (a) 1:0.2, (b) 1:0.4, (c) 1:0.8 and (d) 1:1. (e) relationship between the intensity of the oligomer peak at 436 nm at different pump energies.

are able to produce dual ASE. Herein, the CO produces dual ASE under the influence of MEH-PPV due to the strong interaction between the two materials. The ASE peak at 436 nm coincides with the absorption minimum of the oligomer/MEH-PPV, as shown in Fig. 4 (a). Dual ASE is achieved only in the presence of MEH-PPV, i.e., the oligomer cannot produce ASE at the 0–1 band on its own. Fig. 7 (d) shows the relationship between the intensity of the oligomer peak at 436 nm at different pump energies and different concentration ratios of MEH-PPV. The ASE peak at 436 nm is produced only under the influence of the presence of MEH-PPV. The intensity at 436 nm was almost zero when MEH-PPV is not present in the solution in conjunction with Fig. 6 (a). When a MEH-PPV is added to form a concentration of (1:0.4), the peak appears, and when the pump power increased, it produces a distinctive ASE peak. And for higher pump energies, the intensity of ASE increased sharply, as shown in Fig. 7(d) ii. When more MEH-PPV is added to form a concentration of (1:0.8), the threshold of ASE decreased to 4 mJ; also, with an increase in pump energy, the intensity at 436 nm increases more rapidly, as shown in 8(d) iii.

Fig. 8 (a) shows the TRS spectra of the CO/CP, which has a similar concentration as in Fig. 7 (a). They show a time delay of 1 ns for interaction with the oligomer. The BECV-DHF/MEH-PPV dynamic exchanges can be found using time-resolved studies. Fig. 8 shows that when a small quantity of MEH-PPV (50 μL) is added to the CO solution, the 436 nm peak starts appearing. To exclude the possibility of the 436 nm peak appearing due to a reduction in concentration, 50 μL of toluene was added to the pure oligomer solution, and the TRS spectra showed only one peak at 465 nm, with no trace of the 447 nm band. However, the presence of MEH-PPV altered the spectrum of the oligomer. Additionally, note that the 436 nm peak appears 1 ns later than the appearance of the 464 nm band, whereas the MEH-PPV band appears simultaneously with the 464 nm band of the CO. The simultaneous occurrences of the BECV-DHF/MEH-PPV bands at a concentration of more than 100 μL show that exchange occurs on a much faster time scale than the resolution of the TRS camera.

3.2. Oligomer/MEH-PPV solution in a cavity

To determine the tunability and lasing action of the CO/CP solution, an optical cavity of length 28 ± 10 mm (length tunable) with one mirror of 100% reflectivity and another of 60% reflectivity was designed. The CO/CP solution produces a two-broadband LIF spectrum with two bands, one from 440 to 466 nm and the other from 550 nm to 650 nm. The oligomer is very efficient and able to produce dual ASE at 436 nm and 464 nm in the presence of MEH-PPV. However, the fluorescence band from 550 nm to 650 nm cannot be used to produce ASE for the concentration studied. Without the laser cavity, the broadband from 550 nm to 650 nm cannot be narrowed at these low concentrations of MEH-PPV.

The same CO/CP solution was used in Fig. 9 (a) to (c), which shows the CO/CP spectra in the cavity. The pump energy and relative CO/CP concentration were kept constant. The length of the cavity was varied with the help of the mirror distance. When the length of the cavity is altered by a few mm, the emission wavelength also changes from 560 nm. The fluorescence becomes spectrally narrow, and the divergence of the light beam becomes 15 mrad when the length of the cavity is 28 mm. When the length of the cavity is 30 mm, a single band is observed at approximately 560 nm, with a divergence of 12 mrad. Without the cavity setup, it is impossible to achieve a very intense laser from MEH-PPV at 560 nm. Depending on the length of the cavity, dual peaks at 563 and 574 nm are also achieved. MEH-PPV inherently produces an ASE peak at 575 nm [45], but due to the presence of BECV-DHF, the MEH-PPV peak is blue-shifted to 563 nm. The simple cavity used here allowed us to produce three narrow peaks simultaneously; the ones at 440 nm and 464 nm were developed with the cavity in a single pass, which does not depend on the cavity geometry. However, the sharp peak at 560 nm with an FWHM 6 nm is a laser peak due to the cavity, and

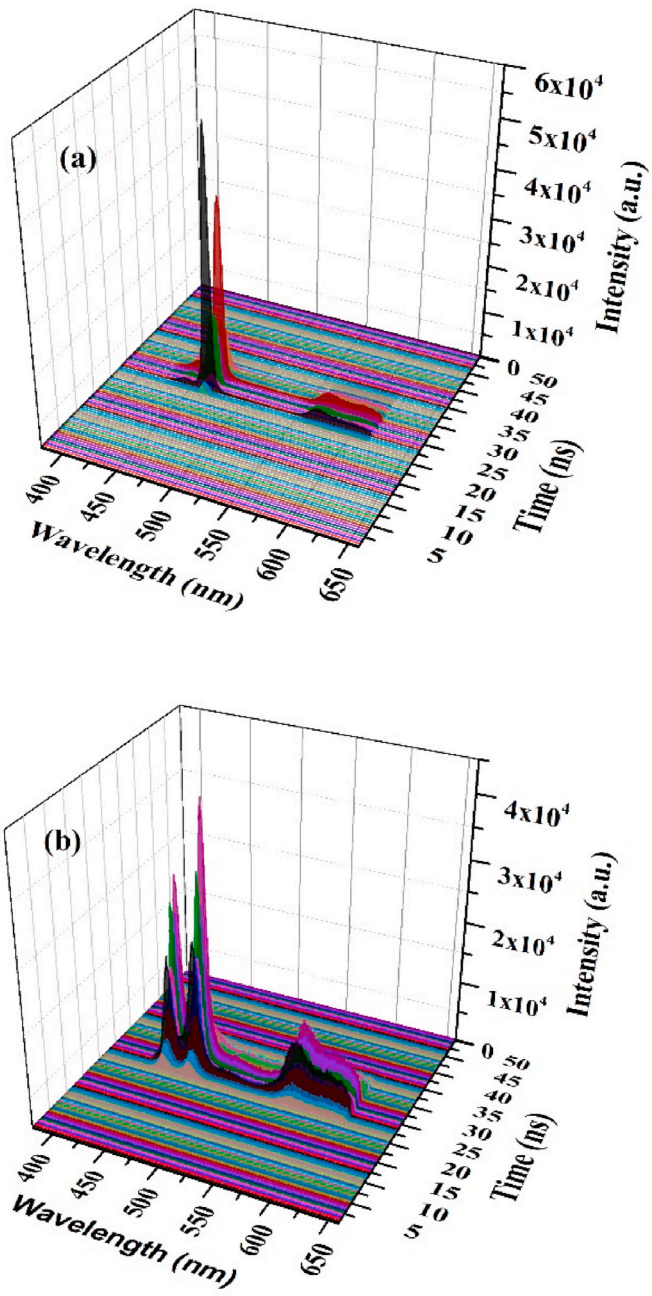

Fig. 8. Time-resolved dynamics of the CO/CP in toluene at pump energy of 8 mJ and ratios of (a) 1:0.2 and (b) 1:0.4.

multiple wavelengths receive feedback; hence, this laser spectrum is quite broad.

The TRS spectra of the CO/CP composite solution are shown in Fig. 10. They show that both MEH-PPV and the CO are in constant competition to be excited by pump photons. The large dip (hole) at approximately 600 nm is due to the attenuation of the cavity. The fluorescence at this band is cut off due to the bandgap cut-off effect. The band beyond 650 nm is the tail fluorescence of MEH-PPV, which is mostly fluorescence net amplified by feedback within the cavity. When the concentrations of MEH-PPV and the CO are sufficiently high, and the pump energy is approximately 8 mJ, the TRS spectra show that ASE of the oligomer and lasing from MEH-PPV are produced simultaneously, and the oligomer produces ASE at 436 nm through the spectral modulation process. This is not altered under the cavity setup. MEH-PPV, instead of producing broadband LIF, produces a sharp laser peak,

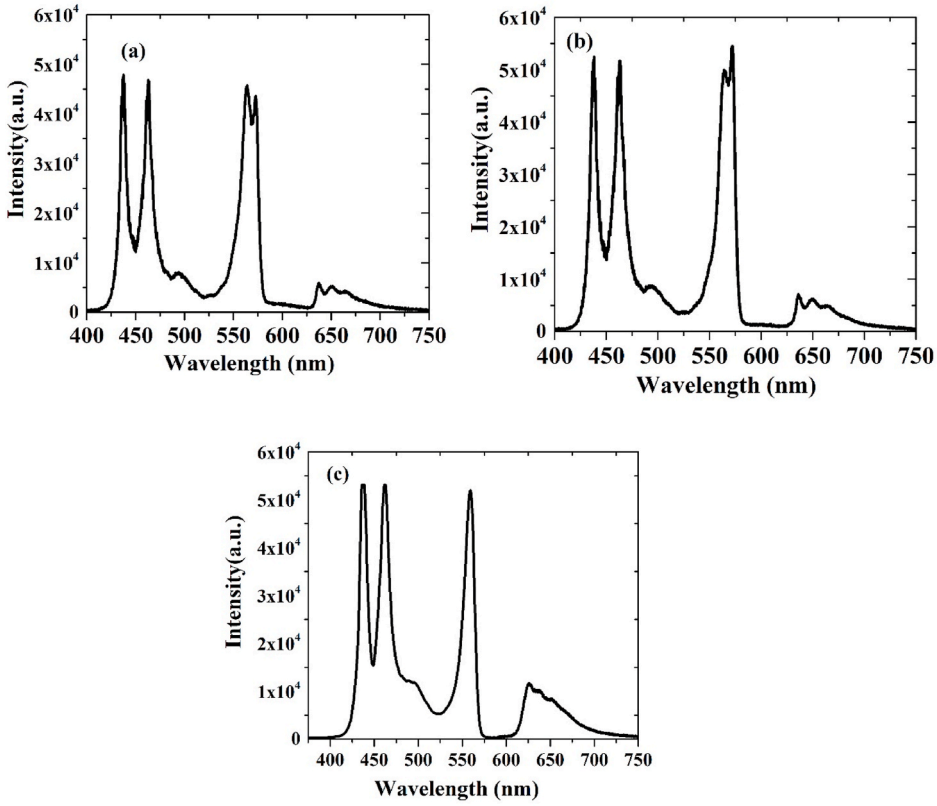

Fig. 9. (a) Laser spectra of BECV-DHF/MEH-PPV blends in toluene at a ratio of 1:0.4. and a 10 mJ pump energy.

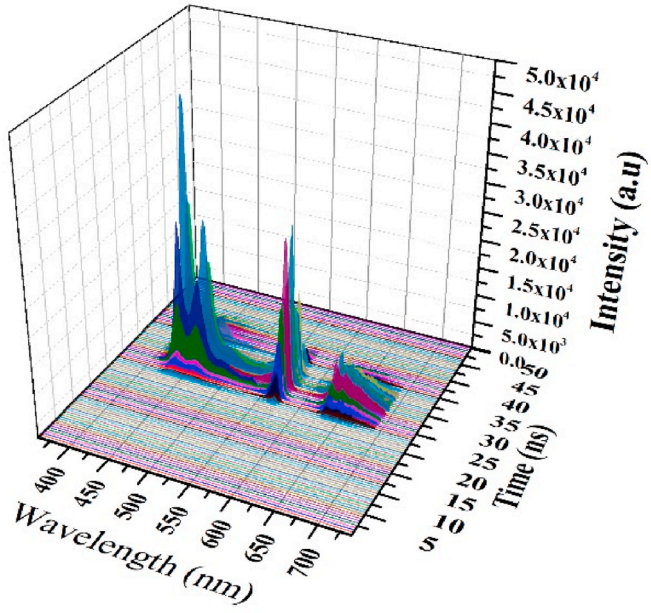

Fig. 10. Time-resolved dynamic lasing of BECV-DHF/MEH-PPV blends in the cavity.

indicating that the cavity does not affect the dynamics of MEH-PPV.

4. Conclusions

The oligomer is forced to produce dual ASE in the presence of MEH-PPV due to the modulation of HOMO-LUMO structure. The new peak of 436 nm appeared as a result of the MEH-PPV that can absorb high at 464 nm. TRS spectra reveal the simultaneous occurrence of oligomer and polymer bands. However, the appearance of the 436 nm band at a low concentration of the CP showed a time delay of 1 ns. The intensity of the 436 nm peak is proportional to the MEH-PPV concentration and pump energy. This phenomenon is used to design a tunable laser using an optical cavity with two mirrors (100% and 60%) and grating with a suitable cavity length. The laser is tunable from 560 nm to 580 nm.

Author contributions

Mohamad S. AlSalhi designed the work. Mamduh J. Aljaafreh, Saradh. perform the experiments, discussed and analysis the results as well as wrote the manuscript. Mohamad S. AlSalhi, reviewed and approved the manuscript.

CRediT authorship contribution statement

Mamduh J. Aljaafreh: Methodology, Software, Data curation, Visualization, Writing - original draft, Investigation, Formal analysis. **Mohamad S. AlSalhi:** Supervision, Writing - review & editing, Resources. **Saradh Prasad:** Conceptualization, Methodology, Software, Writing - original draft, Visualization, Data curation.

Declaration of competing interest

The authors declare that they have no known competing financial interests or personal relationships that could have appeared to influence the work reported in this paper.

Acknowledgments

The authors are grateful to the Deanship of Scientific Research, King Saud University for funding through Deanship of Scientific Research

Chairs.

Appendix A. Supplementary data

Supplementary data to this article can be found online at https://doi.org/10.1016/j.optmat.2020.110575.

References

[1] F. Diederich, R.E. Martin, Linear monodisperse p -conjugated Oligomers : Angew. Chem. Int. Ed. 38 (1999) 1350–1377, https://doi.org/10.1002/(SICI)1521-3773(19990517)38:10<1350::AID-ANIE1350>3.0.CO, 2-6.

[2] K. Müllen, G. Wegner, Electronic Materials: the Oligomer Approach, John Wiley & Sons, 2008.

[3] A.L. Kanibolotsky, I.F. Perepichka, P.J. Skabara, Star-shaped π-conjugated oligomers and their applications in organic electronics and photonics, Chem. Soc. Rev. 39 (2010) 2695–2728, https://doi.org/10.1039/b918154g.

[4] D. Gh, D. Kong, J. Gautrot, S.K. Vootla, Fabrication and characterization of conductive conjugated polymer-coated Antheraea mylitta silk fibroin fibers for biomedical applications, Macromol. Biosci. 17 (2017) 1600443.

[5] E. Radvar, H.S. Azevedo, Supramolecular peptide/polymer hybrid hydrogels for biomedical applications, Macromol. Biosci 19 (2019) 1800221.

[6] A. Kausar, Scope of polymer/graphene nanocomposite in defense relevance: defense application of polymer/graphene. Polym. Nanocomposites Adv. Eng. Mil. Appl., IGI Global, 2019, pp. 296–315.

[7] C. Gilhotra, M. Chander, Sanjay, A review: conducting polyaniline polymer. AIP Conf. Proc., AIP Publishing LLC, 2019, p. 150008.

[8] S. Series, O. Sciences, Organic Solid- State Lasers, n.d.

[9] M. Ann, S. Lattante, R. Cingolani, G. Gigli, G. Barbarella, L. Favaretto, Emission properties of organic random lasers, Phys. Status Solidi C Conf. 1 (2004) 450–453, https://doi.org/10.1002/pssc.200304017.

[10] M. Anni, G. Gigli, R. Cingolani, M. Zavelani-Rossi, C. Gadermaier, G. Lanzani, G. Barbarella, L. Favaretto, Amplified spontaneous emission from a soluble thiophene-based oligomer, Appl. Phys. Lett. 78 (2001) 2679–2681, https://doi.org/10.1063/1.1369392.

[11] W. Lu, G. Tu, B. Zhong, D. Ma, L. Wang, X. Jing, F. Wang, Amplified Spontaneous Emission from a New 4-triarylamine Substituted 1 , 8-naphthalimide Semiconductor Oligomer vol. 409, 2005, pp. 105–109, https://doi.org/10.1016/j.cplett.2005.04.101.

[12] M.A. Díaz-García, M. Morales-Vidal, M.G. Ramírez, J.M. Villalvilla, P.G. Boj, J. A. Quintana, A. Retolaza, S. Merino, Solution-processable, photo-stable, low-threshold, and broadly tunable thin film organic lasers based on novel high-performing laser dyes, Org. Light Emit. Mater. Devices XIX. 9566 (2015) 95660Q, https://doi.org/10.1117/12.2187015.

[13] C.J. Brabec, V. Dyakonov, J. Parisi, N.S. Sariciftci, Organic Photovoltaics: Concepts and Realization, vol. 60, Springer, New York NY USA, 2003.

[14] S. Lattante, M.L. De Giorgi, M. Pasini, M. Anni, Low threshold Amplified Spontaneous Emission properties in deep blue of poly[(9,9-dioctylfluorene-2,7-dyil)-alt-p-phenylene] thin films, Opt. Mater. 72 (2017) 765–768, https://doi.org/10.1016/j.optmat.2017.07.025.

[15] S. Klinkhammer, X. Liu, K. Huska, Y. Shen, S. Vanderheiden, S. Valouch, C. Vannahme, S. Bräse, T. Mappes, U. Lemmer, Continuously tunable solution-processed organic semiconductor DFB lasers pumped by laser diode, Optic Express (2012), https://doi.org/10.1364/oe.20.006357.

[16] S. Chénais, S. Forget, Recent advances in solid-state organic lasers, Polym. Int. 61 (2012) 390–406, https://doi.org/10.1002/pi.3173.

[17] C.R. McNeill, N.C. Greenham, Conjugated-polymer blends for optoelectronics, Adv. Mater. (2009), https://doi.org/10.1002/adma.200900783.

[18] Y. Wang, G. Tsiminis, Y. Yang, A. Ruseckas, A.L. Kanibolotsky, I.F. Perepichka, P. J. Skabara, G.A. Turnbull, I.D.W. Samuel, Broadly tunable deep blue laser based on a star-shaped oligofluorene truxene, Synth. Met. (2010), https://doi.org/10.1016/j.synthmet.2010.04.016.

[19] M.J. Aljaafreh, S. Prasad, M.S. AlSalhi, Z.A. Alahmed, M.M. Al-Mogren, Optically pumped intensive light amplification from a blue oligomer, Polymers 11 (2019), https://doi.org/10.3390/polym11101534.

[20] Y. Lin, X. Zhan, Oligomer molecules for efficient organic photovoltaics, Acc. Chem. Res. 49 (2016) 175–183, https://doi.org/10.1021/acs.accounts.5b00363.

[21] Y. Lin, X. Zhan, Oligomer molecules for efficient organic photovoltaics, Acc. Chem. Res. (2016), https://doi.org/10.1021/acs.accounts.5b00363.

[22] Y. Liu, K. Zhang, Y. Li, Q. Wei, Y. Bo, L. Wang, Y. Qian, R. Xia, Q. Zhang, W. Huang, Low–threshold sky-blue gain medium from a Triazine-capped ladder-type oligomer neat film, Org. Electron. 76 (2020), https://doi.org/10.1016/j.orgel.2019.105452.

[23] H.H. Fang, R. Ding, S.Y. Lu, J. Yang, X.L. Zhang, R. Yang, J. Feng, Q.D. Chen, J. F. Song, H.B. Sun, Distributed feedback lasers based on thiophene/phenylene co-oligomer single crystals, Adv. Funct. Mater. 22 (2012) 33–38, https://doi.org/10.1002/adfm.201101467.

[24] Q.D. Zhang, B. Piro, V. Noël, S. Reisberg, N. Serradji, C.Z. Dong, F. Mameche, M. C. Pham, An electroactive conjugated oligomer for a direct electrochemical DNA sensor, Synth. Met. 162 (2012) 1496–1502.

[25] M.J. Aljaafreh, S. Prasad, M.S. AlSalhi, Z.A. Alahmed, Ultrafast dynamics of laser from green conjugated-oligomer in solution, Polymer 169 (2019) 106–114, https://doi.org/10.1016/j.polymer.2019.02.022.

[26] J. Herr, G. Richard, RSC Adv. Sens. 6 (2013) 7, https://doi.org/10.1039/d0ra04742b.

[27] Y. Zhang, Z. Xu, Direct observation of the size dependence of Dexter energy transfer from polymer to small PbS quantum dots, Appl. Phys. Lett. 93 (2008) 83106.

[28] B. Liu, B.S. Gaylord, S. Wang, G.C. Bazan, Effect of chromophore-charge distance on the energy transfer properties of water-soluble conjugated oligomers, J. Am. Chem. Soc. 125 (2003) 6705–6714, https://doi.org/10.1021/ja028961w.

[29] S. Complexation, B.M. Stork, B.S. Gaylord, A.J. Heeger, G.C. Bazan, Stork_et_al-2002-Advanced_Materials, 2002, pp. 361–366, 0.

[30] X. Yang, T.E. Dykstra, G.D. Scholes, Photon-echo studies of collective absorption and dynamic localization of excitation in conjugated polymers and oligomers, Phys. Rev. B Condens. Matter 71 (2005) 1–15, https://doi.org/10.1103/PhysRevB.71.045203.

[31] S.M. Aly, C.L. Ho, D. Fortin, W.Y. Wong, A.S. Abd-El-Aziz, P.D. Harvey, Intrachain electron and energy transfer in conjugated organometallic oligomers and polymers, Chem. Eur J. 14 (2008) 8341–8352, https://doi.org/10.1002/chem.200800304.

[32] D. Sengottuvelu, V. Kachwal, P. Raichure, T. Raghav, I.R. Laskar, Aggregation-induced enhanced emission (AIEE) active conjugated mesoporous oligomers (CMOs) with improved quantum yield and low-cost trace nitro aromatic explosives detection, ACS Appl. Mater. Interfaces (2020), 0c05273, https://doi.org/10.1021/acsami.0c05273 acsami.

[33] D. Gao, Z. Wang, B. Liu, L. Ni, M. Wu, Z. Zhang, Resonance energy transfer-amplifying fluorescence quenching at the surface of silica nanoparticles toward ultrasensitive detection of TNT, Anal. Chem. 80 (2008) 8545–8553, https://doi.org/10.1021/ac8014356.

[34] A. Kovach, J. He, P.J.G. Saris, D. Chen, A.M. Armani, Optically tunable microresonator using an azobenzene monolayer, AIP Adv. 10 (2020) 45117.

[35] V.V. Jerca, F.A. Jerca, I. Rau, A.M. Manea, D.M. Vuluga, F. Kajzar, Advances in understanding the photoresponsive behavior of azobenzenes substituted with strong electron withdrawing groups, Opt. Mater. 48 (2015) 160–164.

[36] L.M. Goldenberg, V. Lisinetskii, S. Schrader, Azobenzene lasers tuned over a 200 nm range, Adv. Opt. Mater. 1 (2013) 527–533.

[37] M.C. Spiridon, K. Iliopoulos, F.A. Jerca, V.V. Jerca, D.M. Vuluga, D.S. Vasilescu, D. Gindre, B. Sahraoui, Novel pendant azobenzene/polymer systems for second harmonic generation and optical data storage, Dyes Pigments 114 (2015) 24–32.

[38] F.A. Jerca, V.V. Jerca, D.F. Anghel, G. Stinga, G. Marton, D.S. Vasilescu, D. M. Vuluga, Novel aspects regarding the photochemistry of azo-derivatives substituted with strong acceptor groups, J. Phys. Chem. C 119 (2015) 10538–10549.

[39] F.A. Jerca, V.V. Jerca, F. Kajzar, A.M. Manea, I. Rau, D.M. Vuluga, Simultaneous two and three photon resonant enhancement of third-order NLO susceptibility in an azo-dye functionalized polymer film, Phys. Chem. Chem. Phys. 15 (2013) 7060–7063.

[40] M. Anni, Poly [2-methoxy-5-(2-ethylhexyloxy)-1, 4-phenylenevinylene](MeH-PPV) amplified spontaneous emission optimization in poly (9, 9-dioctylfluorene (PFO)): MeH-PPV active blends, J. Lumin. 215 (2019) 116680.

[41] M. Frisch, G.W. Trucks, H.B. Schlegel, G.E. Scuseria, M.A. Robb, J.R. Cheeseman, G. Scalmani, V. Barone, B. Mennucci, Ga Petersson, Gaussian 09, Revision D. 01, Gaussian, Inc., Wallingford CT, 2009, p. 201.

[42] A.L. Holt, J.M. Leger, S.A. Carter, Electrochemical and optical characterization of p- and n-doped poly[2-methoxy-5-(2-ethylhexyloxy)-1,4-phenylenevinylene], J. Chem. Phys. 123 (2005), https://doi.org/10.1063/1.1949188.

[43] M. Fakis, I. Polyzos, G. Tsigaridas, V. Giannetas, P. Persephonis, I. Spiliopoulos, J. Mikroyannidis, Dual amplified spontaneous emission and laser action from a model oligo(phenylene vinylene): comparison with the corresponding polymer, Opt. Mater. 27 (2004) 503–507, https://doi.org/10.1016/j.optmat.2004.03.016.

[44] M. Anni, Dual band amplified spontaneous emission in the blue in Poly(9,9-dioctylfluorene) thin films with phase separated glassy and β-phases, Opt. Mater. 96 (2019), https://doi.org/10.1016/j.optmat.2019.109313.

[45] K.H. Ibnaouf, Influence of the CdSe quantum dots concentration on the amplified spontaneous emission from the conjugated polymer (MEH-PPV) in solution, Optic Laser. Technol. 67 (2015) 150–154, https://doi.org/10.1016/j.optlastec.2014.10.008.